HEAT TRANSFER SIMULATION AND PERFORMANCE OPTIMIZATION OF PLATE-TYPE PHASE CHANGE ENERGY STORAGE UNIT

Long MIAO[1], Rui WAN[*2, 3], Zhen LIU[2, 3], Huawei WU[2, 3]

[1]School of Mechanical & Electrical Engineering, Xuzhou University of Technology, Jiangsu 221000, China

[*2]Hubei Key Laboratory of Power System Design and Test for Electrical Vehicle, Hubei University of Arts and Science, Xiangyang 441053, China

[3]School of Automotive and Traffic Engineering，Hubei University of Arts and Science, Xiangyang 441053, China

[*]Corresponding author; E-mail: wanrui7035@163.com

As the core of the phase change energy storage technology, the heat transfer performance of the phase change energy storage unit has an important impact on the operating efficiency of the energy storage system. In this study, a three-dimensional CFD model of the plate-type phase change energy storage unit is established to simulate the melting process of paraffin wax. Three types of plate-type phase change energy storage unit models are established, without fins, single fin, and double fins. The influence of cylindrical fin on natural convection melting process of paraffin is studied, which provides the basis for the design and performance optimization of plate-type phase change energy storage unit, and improve its application value. The results show that the melting time of paraffin in the energy storage unit without fins is 858 s, and the melting time is shortened to 827 ~ 842 s after adding single fin. The melting time of paraffin wax with single fin is lower than that with double fins. For the plate-type phase change energy storage unit, adding fins at the central section can effectively improve the melting rate of phase change material. The single fin A located at the lower part of the central section has the greatest promotion effect on paraffin melting. The key to enhance the phase change heat transfer process in plate-type phase change energy storage unit is the paraffin in the lower half of the symmetry plane.

Key words: *plate-type phase change energy storage unit, fins, paraffin wax, natural convection, numerical simulation*

1. Introduction

In the process of development and utilization of various energy sources, there are often certain temporal and spatial differences between energy supply and demand, such as the peak-valley difference of grid load. For renewable energy sources such as wind, solar and tidal energy, there is greater volatility in energy supply and greater imbalance between energy supply and demand. Solid-liquid phase change energy storage technology has the advantages of high heat storage density,

good equipment compactness and easy management, which can effectively improve the volatility of energy supply and enhance the stability of energy supply [1, 2]. Phase change energy storage technology has been widely used in buildings [3], solar heating systems [4, 5], waste heat recovery systems [6, 7] and air conditioning systems [8, 9].

As the core of phase change energy storage technology, the heat transfer performance of phase change energy storage unit has an important impact on the operating efficiency of energy storage system. Plate-type phase change energy storage units (P-PCESU) and shell and tube phase change energy storage units are the most commonly used forms of phase change energy storage units [10, 11]. The enhancement of heat transfer performance of the P-PCESU has attracted the attention of some researchers. Zhou et al. [12] designed a cascade phase change heat storage model and numerically simulated its internal heat transfer process. The results showed that the position of the phase change material had a significant impact on the heat transfer characteristics, and the convective heat transfer between the lower and middle phase change materials played a key role in the overall melting rate of the heat storage unit.

The current research hotspot for enhancing heat transfer in energy storage units is to add materials with strong thermal conductivity to substrates such as paraffin to prepare composite phase change materials. Yang et al. [13] prepared a metal foam-paraffin composite phase change material, and experimentally studied its phase change heat transfer process. The results show that the uniformity of the internal temperature distribution of the composites is improved, the heat flux is significantly increased, and the poor heat transfer performance of the bottom during the melting process of pure paraffin wax is improved. Wang et al. [14] studied the melting solidification cycle process of composite phase change materials using visual experimental methods. The results show that the composite phase change material can help to improve the latent heat storage capacity and increase the total heat storage of the heat storage unit. Shafee et al. [15] studied the heat release process during water solidification, and added copper oxide particles to the water to prepare nanoparticle-reinforced phase change materials. With the increase of nanomaterial concentration, the solidification time tends to decrease. The results show that the addition of copper oxide nanopowder reduces the solidification time by 14.39%.

Structural optimization of phase change heat transfer units is also an important research direction. Kamkari et al. [16] studied the melting process of phase change materials in rectangular containers with different inclination angles, and the results showed that the inclination of the shell has a significant effect on the formation of natural convection, and therefore also has a great influence on the heat transfer rate and melting time of phase change materials. Gurel [17] studied the P-PCESU made of corrugated steel plate and compared it with the performance of the cylindrical energy storage unit, and found that the phase change material in the plate phase change energy storage unit has a short solidification time, reducing the solidification time by up to 63%. Lin et al. [18] proposed a new P-PCESU, in which a distributed water flow channel is provided in the substrate for charging or discharging the phase change material. The experimental results show that the pillow plate type heat exchanger has good compactness and heat transfer performance. Liu et al. [9] experimentally studied the P-PCESU with different geometric structures, analyzed the influence of thermocouple position and unit aspect ratio on paraffin melting rate, and proposed an optimized size with an aspect ratio of 3:1 and a thickness of 30 mm.

In the published research, on the one hand, the composite phase change material is prepared by adding enhanced heat transfer materials to the paraffin substrate, and on the other hand, the P-PCESU itself is studied to optimize its structure and enhance the heat transfer performance inside the energy storage unit. In this study, a three-dimensional CFD model of the P-PCESU is established, and the melting process of paraffin in the P-PCESU is simulated and analyzed. Then, cylindrical ribs are added to P-PCESU, and the influence of cylindrical ribs on the natural convective melting process of paraffin is studied, and the number and distribution of ribs are optimized, so as to improve the heat transfer performance of P-PCESU, which provides a basis for the performance optimization of P-PCESU.

2 Simulation model

2.1 Physical model

The phase change energy storage unit in this study is a flat plate type, with aluminum as the outer shell material and paraffin as the internal filling material. The structure of the energy storage unit is shown in Fig. 1.

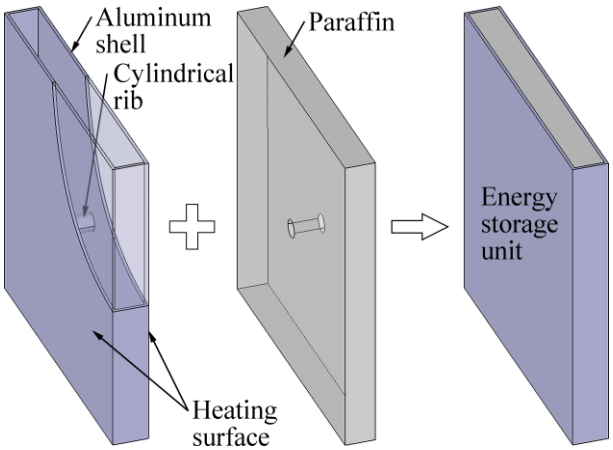

Fig.1 Plate-type phase change energy storage unit

The volume of paraffin is 100 × 100 × 10 mm^3, and the thickness of the aluminum shell is 1 mm. The energy storage unit has heating surfaces on both sides, which heat the internal paraffin to melt it. In order to enhance the heat transfer performance of the energy storage unit, cylindrical ribs are added in the cavity to compare and study the strengthening effect of different numbers and arrangement of ribs on the heat transfer performance of the energy storage unit.

The cylindrical ribs in the energy storage unit are divided into two groups, single ribs and double ribs, and each group has three different rib arrangements. The diameter of the single rib is 6 mm, the diameter of each rib in the double rib group is 4.25 mm, and the total volume of the ribs is the same. The single rib is located in the center section of the energy storage unit, while the double rib is symmetrically distributed on both sides of the center section. In the simulation process, four temperature monitoring points are set in the energy storage unit, and the measurement points are located on the symmetrical surface of the energy storage unit. The location of the ribs and temperature measurement points is shown in Fig. 2 in millimeters.

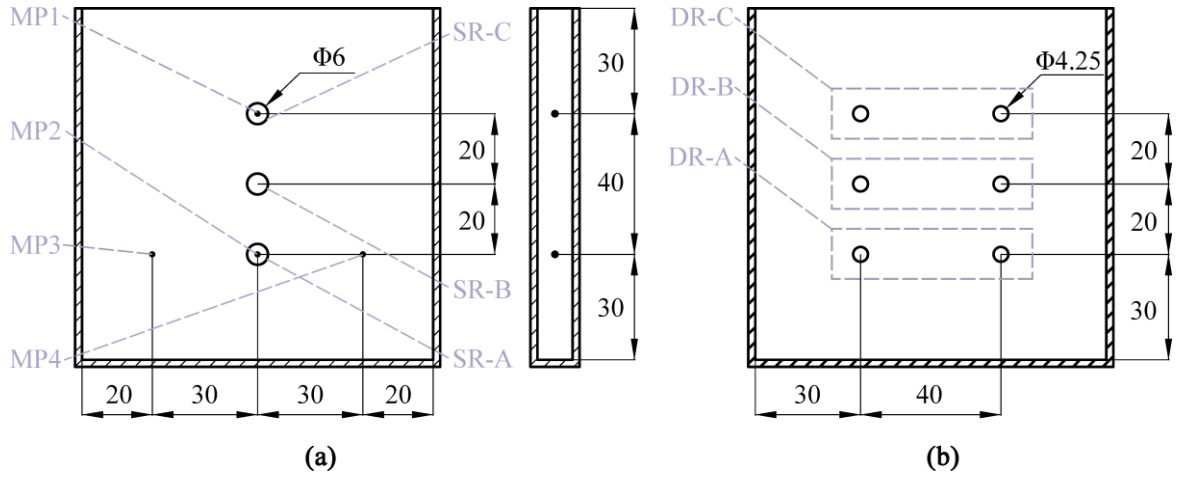

Fig.2 Location of ribs and temperature measurement points (MP): (a) Single rib (SR); (b) Double ribs (DR)

2.2 Mathematical model

The melting process of paraffin belongs to the problem of phase change heat transfer, and the solid-liquid interface during the melting process is a region where two phases coexist. The density of solid paraffin wax decreases after melting, and natural convection occurs in high-temperature liquid paraffin wax under the effect of buoyancy. The enthalpy porosity method [19, 20] is applied to simulate the melting process of paraffin, and the liquid fraction parameter was used to describe the changes in the solid-liquid interface. The control equations are as follows:

$$\frac{\partial \rho}{\partial t}+\frac{\partial(\rho u)}{\partial x}+\frac{\partial(\rho v)}{\partial y}+\frac{\partial(\rho w)}{\partial z}=0 \tag{1}$$

$$\begin{cases}\rho\left(\dfrac{\partial u}{\partial t}+u\dfrac{\partial u}{\partial x}+v\dfrac{\partial u}{\partial y}+w\dfrac{\partial u}{\partial z}\right)=\mu\left(\dfrac{\partial^2 u}{\partial x^2}+\dfrac{\partial^2 u}{\partial y^2}+\dfrac{\partial^2 u}{\partial z^2}\right)-\dfrac{\partial p}{\partial x}+S_u \\ \rho\left(\dfrac{\partial v}{\partial t}+u\dfrac{\partial v}{\partial x}+v\dfrac{\partial v}{\partial y}+w\dfrac{\partial v}{\partial z}\right)=\mu\left(\dfrac{\partial^2 v}{\partial x^2}+\dfrac{\partial^2 v}{\partial y^2}+\dfrac{\partial^2 v}{\partial z^2}\right)-\dfrac{\partial p}{\partial y}+S_v \\ \rho\left(\dfrac{\partial w}{\partial t}+u\dfrac{\partial w}{\partial x}+v\dfrac{\partial w}{\partial y}+w\dfrac{\partial w}{\partial z}\right)=\mu\left(\dfrac{\partial^2 w}{\partial x^2}+\dfrac{\partial^2 w}{\partial y^2}+\dfrac{\partial^2 w}{\partial z^2}\right)-\dfrac{\partial p}{\partial z}+S_w\end{cases} \tag{2}$$

$$\rho\left(\frac{\partial H}{\partial t}+u\frac{\partial H}{\partial x}+v\frac{\partial H}{\partial y}+w\frac{\partial H}{\partial z}\right)=\frac{\lambda}{c_p}\left(\frac{\partial^2 H}{\partial x^2}+\frac{\partial^2 H}{\partial y^2}+\frac{\partial^2 H}{\partial z^2}\right)+S_h \tag{3}$$

In the above equations, u, v, and w are the components of velocity in the x, y, and z directions, respectively; ρ is the density of paraffin wax ($kg \cdot m^{-3}$); μ is the dynamic viscosity of paraffin wax ($Pa \cdot s$); λ *i*s the thermal conductivity of paraffin wax ($W \cdot m^{-1} K^{-1}$); c_p is the specific heat capacity of paraffin ($kJ \cdot kg^{-1} \cdot K^{-1}$); p is the pressure (Pa); S_u, S_v, and S_w are the source terms of the momentum equation in the x, y, and z directions, respectively; S_h is the source term of the energy equation.

The enthalpy equation is:

$$\begin{cases} H = h + \Delta H \\ h = h_{ref} + \int_{T_{ref}}^{T} c_p \mathrm{d}T \\ \Delta H = \beta L \end{cases} \tag{4}$$

Among them, H is the specific enthalpy (kJ·kg^{-1}), and h is the sensible enthalpy (kJ·kg^{-1}), ΔH is the latent enthalpy (kJ·kg^{-1}); L is the latent heat of phase transition of paraffin (kJ·kg^{-1}); T_{ref} is the reference temperature (K); H_{ref} is the enthalpy at the reference temperature (kJ·kg^{-1}); β is the volume fraction of liquid paraffin; T_{l} is the liquidus temperature of the material (K); T_{s} is the solidus temperature of the material (K).

3 Simulation Method

The P-PCESU shown in Fig. 1 is meshed. Poly-Hexcore grid is generated using Fluent meshing. In order to verify the independence of the grid, the calculation domain is divided into 40000–500000 grids, and simulation calculations are conducted for 500 seconds under the same boundary conditions. The temperature variations at measurement points 1 and 2 are shown in Table 1. After the number of grids exceeds 250000, the calculation results tend to stabilize. Taking into account the accuracy and time of the calculation, a grid division scheme with a grid number of 250000 was selected.

Table 1 Grid independence verification

Grid number ($\times 10^3$)	40	80	160	250	500
Temperature of MP1 (K)	324.859	325.244	325.452	325.597	325.648
Temperature of MP2 (K)	324.768	325.018	325.256	325.465	325.527

During the calculation process, the heating surfaces on both sides of the energy storage unit are set as constant temperature surfaces, with a heating temperature of 343 K. The other surfaces are insulated walls. The initial temperature of the energy storage unit is 293 K. During the calculation process, the influence of gravity is considered, and the direction of gravity is the negative z-axis.

In the process of numerical simulation, a three-dimensional discrete, implicit unsteady state solver is used to solve the problem. The time step for simulation calculation is 1 second. The convergence criteria are continuity, residual of momentum equation, and energy equation, with thresholds of 10^{-3}, 10^{-3}, and 10^{-6}, respectively. The energy equation and solidification/melting model were loaded during the simulation process. The SIMPLE algorithm is used for the coupling of pressure and velocity. The numerical simulation was conducted using commercial software Ansys Fluent, version R2021.

The phase change material is paraffin, and its physical properties are shown in Table 2. The housing material of the energy storage unit is aluminum, the thermal conductivity is 202.4 W·m^{-1}·K^{-1}, the density is 2719 kg·m^{-3}, and the specific heat capacity is 871 J·kg^{-1}·K^{-1}. In order to consider natural convection, Boussinesq hypothesis is adopted for paraffin density. In the solid-liquid mixing zone, the thermal conductivity and specific heat capacity of paraffin are treated as functions of temperature, and the expressions are:

$$c_p = \begin{cases} 2464 & T < T_s \\ 162T - 50186 & T_s < T < T_l \\ 2950 & T > T_l \end{cases} \quad (5)$$

$$\lambda = \begin{cases} 0.28 & T < T_s \\ -0.0467T + 15.457 & T_s < T < T_l \\ 0.14 & T > T_l \end{cases} \quad (6)$$

Table 2 Physical properties of paraffin

Physical properties	unit	value
Solid specific heat capacity $c_{p,s}$	$J \cdot kg^{-1} \cdot K^{-1}$	2464
Liquid specific heat capacity $c_{p,l}$	$J \cdot kg^{-1} \cdot K^{-1}$	2950
Solid state density ρ_s	$kg \cdot m^{-3}$	900
Liquid density ρ_l	$kg \cdot m^{-3}$	773
Thermal expansion coefficient α	K^{-1}	0.001
Dynamic viscosity μ	Pa·s	0.03
Solid state thermal conductivity λ_s	$W \cdot m^{-1} \cdot K^{-1}$	0.28
Liquid thermal conductivity λ_l	$W \cdot m^{-1} \cdot K^{-1}$	0.14
Solidus temperature T_s	K	325
Liquidus temperature T_l	K	328
Latent heat L	$kJ \cdot kg^{-1}$	205.6

In order to verify the accuracy of the simulation method, the P-PCESU A3 and A5 from reference [9] are modeled and simulated, and the simulation boundary conditions were the same as in the experiment. The comparison of the temperature variation is shown in Fig. 3. The simulation results of A3 and A5 are both consistent with the experimental data trends. The maximum relative error of A3 is 5.3%, and that of A5 is 6.7%. The accuracy of the simulation model calculation results is good, which can be used for subsequent simulation research.

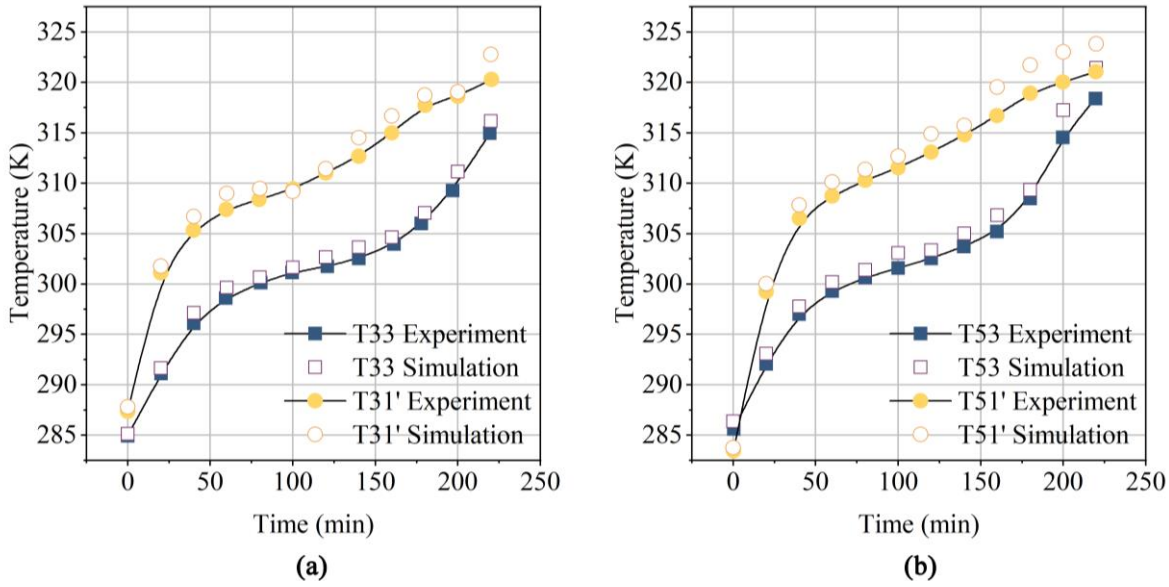

Fig.3 Comparison of simulation results and experimental data: (a) plate configuration A3; (b) plate configuration A5

4 Results and discussion

4.1 Ribless

Firstly, the melting of paraffin without ribs is simulated and analyzed. Fig. 4 shows the variation of the volume fraction of liquid paraffin in the symmetrical plane of the P-PCESU over time. The upper part of the paraffin in the energy storage unit melts quickly and has been completely melted after heating for 600 s. Because the molten paraffin flows upward under the action of natural convection, the melting rate of the paraffin in the upper part is accelerated. The paraffin in the lower half of the energy storage unit has not yet melted after heating for 800 s.

The average Nusselt number $\overline{Nu}$ during melting is [21]:

$$\overline{Nu} = \frac{\rho_l L W_{pcm} H_{pcm} \left(d\beta / d\tau \right)}{\left(t_w - t_m \right) \lambda_l} \tag{7}$$

where W_{pcm} is the width of the phase change element (m); H_{pcm} is the height of the phase change unit (m); t_{w} is the heating wall temperature (K); t_{m} is the melting point of paraffin (K).

Fig. 5 shows the average *Nu* calculated by Eq. (7) and liquid paraffin volume fraction over time. The average *Nu* decreases sharply over time, and then slowly decreases. Because in the early stage of heating, the main heat transfer mechanism inside the energy storage unit is heat conduction, and the thermal resistance increases with the increase of volume fraction of liquid paraffin, resulting in a sharp decrease in *Nu*. With the increase of liquid paraffin, natural convection in the energy storage unit gradually dominates, but the heat transfer enhancement caused by natural convection is weaker than the heat transfer hindrance combined by the increase of thermal resistance and the decrease of heat transfer temperature difference, so the average *Nu* decreases slowly.

The liquid volume fraction in the energy storage unit gradually increases with the heating process, and the liquid volume fraction reaches 1 at 855 s, that is, the paraffin in the energy storage unit is completely melted. The variation trend of liquid volume fraction in the symmetric plane is the same, but at the same time, it is lower than the overall liquid volume fraction. Because the paraffin in the symmetrical plane is far from the heating surface, the melting rate is slow. The volume fraction of liquid paraffin in the symmetrical surface reaches 0.96 after heating for 800 s, and the liquid volume fraction in the entire energy storage unit is 0.98.

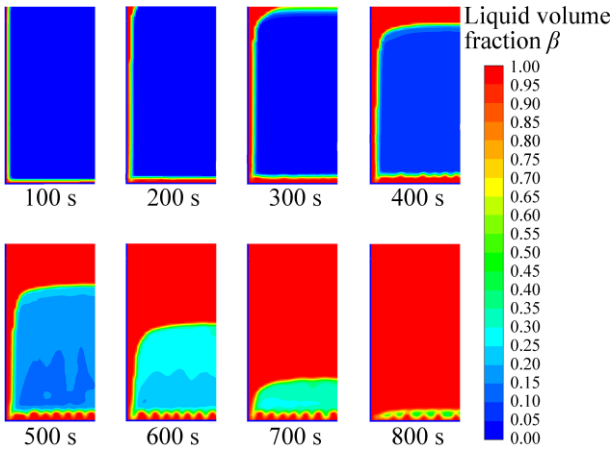

Fig.4 Contour plot of liquid volume fraction without fins

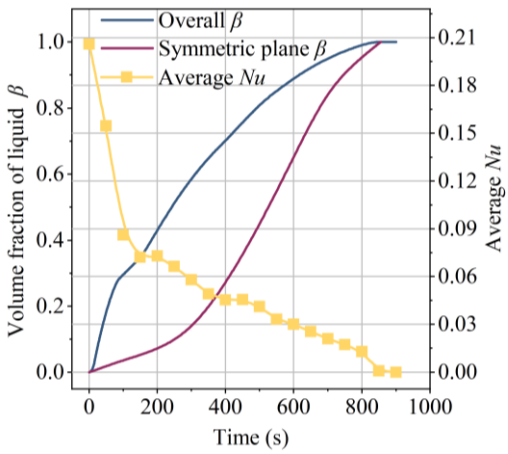

Fig.5 Average *Nu* and liquid paraffin volume fraction

4.2 Single rib

A single cylindrical rib with a diameter of 6 mm and a rib position height of 30 mm, 50 mm and 70 mm is added to the energy storage unit. The effect of ribs in different positions on the liquid volume fraction of the melting process is shown in Fig. 6.

400 s after the heating starts, the paraffin around the ribs is partially melted, and the proportion of liquid paraffin wax is higher than when there are no ribs. At 500 s, the paraffin around the ribs melts further, forming a liquid paraffin area in the middle of the solid paraffin. Due to natural convection, paraffin above the ribs melts faster than those below the ribs. Single rib (SR) A is located in the lower part of the energy storage unit, which heats the paraffin wax that melts slowly in this area, which effectively increases the melting rate of paraffin in the energy storage unit. At 600 s and 800 s, the unmelted paraffin of SR-A is less than that of the other two rib arrangements. The time required for paraffin to melt completely is 827 s for SR-A, 835 s for SR-B, and 842 s for SR-C. Therefore, when the position of the ribs is low, the melting speed of paraffin in the energy storage unit is greatly increased. The melting time of all three groups of single ribs is lower than that of no ribs, because the presence of ribs increases the heat exchange area and makes the internal heating of paraffin wax more uniform.

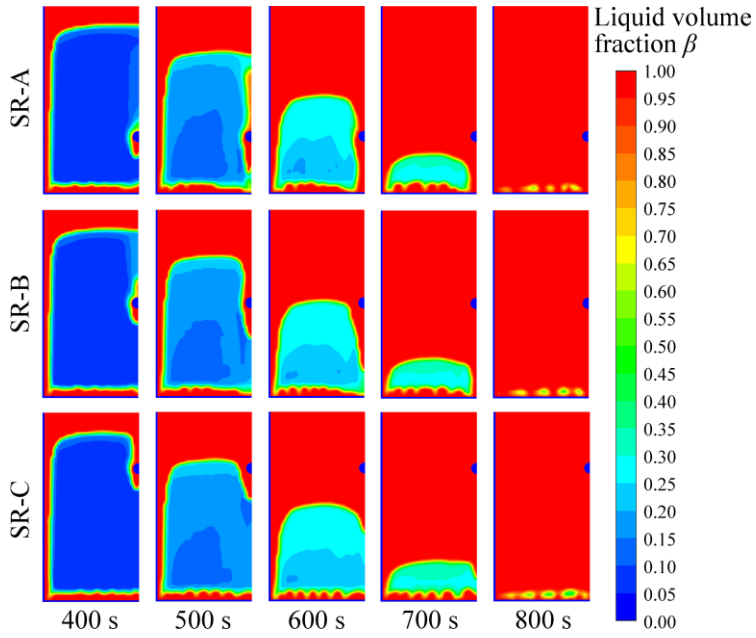

Fig.6 Variation of liquid volume fraction with single fin

Fig. 7 shows the temperature variation at the measuring points (MP1, MP3). MP1 is located in the upper part of the energy storage unit, and the distance between the positions of single ribs A, B and C and MP1 decreases sequentially, so the MP1 of SR-A melts at the latest. The MP1 of SR-C overlaps the position of the rib, so its temperature rises rapidly after the heating starts and remains consistent with the heating surface temperature. After heating for 510 s, the temperature of MP1 in SR-A rises to 328 K, and the paraffin at the corresponding position completely melts. Subsequently, it rapidly heats up under the convection heat transfer of liquid paraffin; The temperature of MP1 of SR-B increased to 328 K after heating for 450 s, and the subsequent heating rate was lower than that of SR-A.

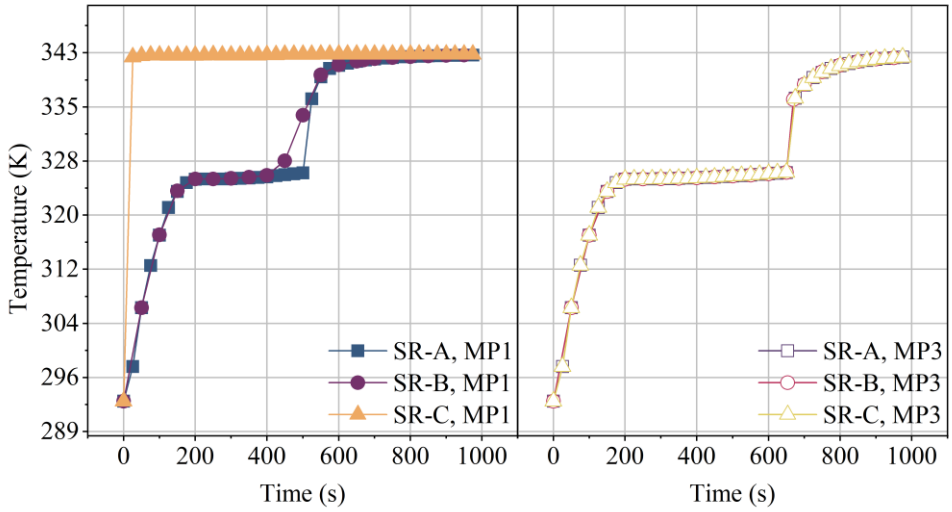

Fig.7 Temperature variation of measuring point with single fin

4.3 Double ribs

Fig. 8 shows the effect of double ribs on the liquid volume fraction. Similar to the situation of the single-rib group, after 500 s of heating, the liquid volume fraction in the energy storage unit is DR-A> DR-B> DR-C, and the lower ribs had a better effect on paraffin melting. When heated for 600 s, the solid paraffin wax at the bottom of DR-A and DR-B has been divided by liquid paraffin, while the unmelted paraffin is still connected in DR-C, and the melting rate is significantly lower than that of the other two rib arrangement. It is worth noting that compared with the single rib group, the unmelted area at 800 s in the double rib group is larger. Because the single rib is located on the central surface of the energy storage unit, it is able to heat the paraffin wax that melts the slowest. The ribs of the double-ribbed group are distributed symmetrically along the center of the energy storage unit, which reduces the heating effect. The total melting time of DR-A, DR-B and DR-C is 843, 849 and 858 s, respectively.

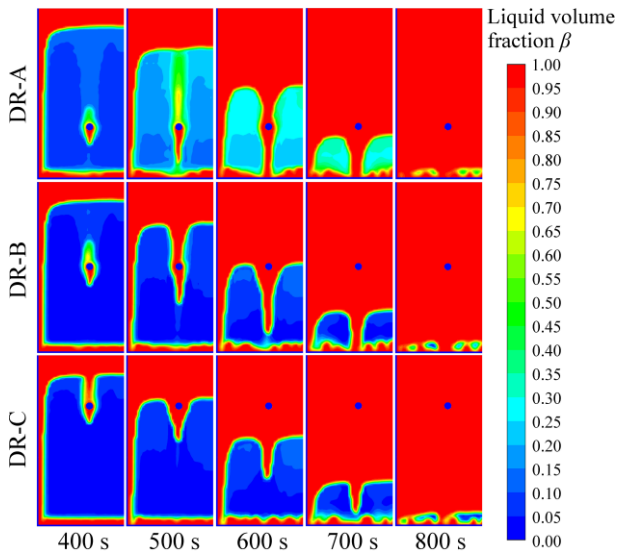

Fig.8 Variation of liquid volume fraction with double fins

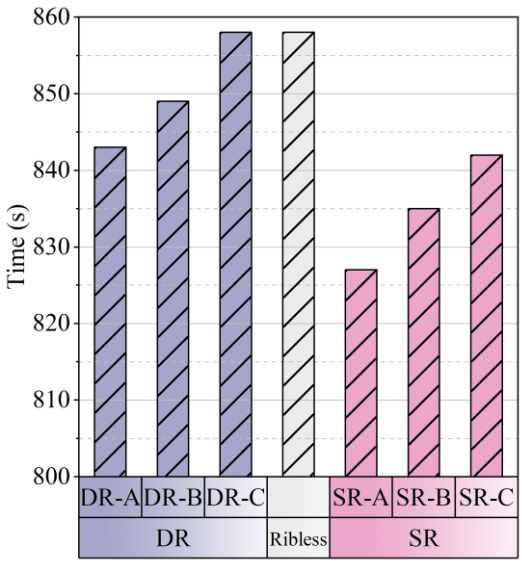

Fig.9 Paraffin melting time

The melting time of paraffin wax with different rib arrangements is shown in Fig. 9. The melting time of DR-C is the same as that without ribs, and the other five rib arrangements all reduce the time for complete melting of paraffin. The melting time of the single rib group is lower than that of the double rib group, indicating that for the P-PCESU, the key to improving the melting speed is to promote the melting of paraffin in the symmetrical plane, especially in the lower half of the symmetrical plane.

5 Conclusions

This article establishes a simulation model for a plate type phase change energy storage unit, verifies the accuracy of the model, and uses it to simulate and study the paraffin phase change heat transfer process. The research results of this article can guide the design and performance optimization of P-PCESU, and improve its application value. The relevant conclusions are as follows:

1) When there are no ribs, the melting time of paraffin in the P-PCESU is 858 s. The average *Nu* in the energy storage unit decreases sharply with the increase of liquid volume fraction, and then slowly decreases. The melting time after adding a single rib is 827–842 s, and the melting time after adding a double rib is 843–858 s. The rib has a promoting effect on the melting of paraffin in the phase change energy storage unit.

2) The melting time of the single-rib group is lower than that of the double-rib group, so adding ribs at the central section of the plate phase change energy storage unit can effectively improve the melting speed of the phase change material.

3) Single rib A located below the center section of the energy storage unit has the greatest effect on paraffin melting. To strengthen the phase change heat transfer process in the plate phase change energy storage unit, the key is to strengthen the heat conduction and natural convection in the lower half of the symmetrical surface.

Acknowledgements

This Work is supported by the Special Fund of Hubei Longzhong Laboratory of Xiangyang Science and Technology Plan, the Hubei Natural Science Foundation Innovation and Development Joint Fund Project (2022CFD083), the Key program of Xiangyang Technology project (High Tech Field) (2021ABH004233), and Distinctive Discipline Group of “New Energy Vehicle and Smart Transportation”.

Nomenclature

c_p	specific heat capacity of paraffin [kJ·kg^{-1}·K^{-1}]	T_l	liquidus temperature of the material [K]
L	latent heat of phase transition of paraffin [kJ·kg^{-1}]	T_{ref}	reference temperature [K]
H	specific enthalpy [kJ·kg^{-1}]	T_s	solidus temperature [K] of the material
h	the sensible enthalpy [kJ·kg^{-1}]	u	components of velocity in x direction [m/s]
H_{ref}	enthalpy at the reference temperature [kJ·kg^{-1}]	v	components of velocity in y direction [m/s]

H_{pcm}	height of the phase change unit [m]	w	components of velocity in z direction [m/s]
ΔH	latent enthalpy [kJ·kg^{-1}]	W_{pcm}	width of the phase change element [m]
Nu	Nusselt number		Greek letters
p	pressure [Pa]	α	thermal expansion coefficient [K^{-1}]
S_u	source terms of the momentum equation in x direction	β	volume fraction of liquid paraffin
S_v	source terms of the momentum equation in y direction	λ	thermal conductivity of paraffin wax [W·m^{-1} K^{-1}]
S_w	source terms of the momentum equation in z direction	μ	dynamic viscosity of paraffin wax [Pa·s]
S_h	source term of the energy equation	ρ	density of paraffin wax [kg·m^{-3}]

References

[1] Zong, H., *et al*., Numerical simulation on the thermal performance of the cascade stage latent thermal storage system with the various phase change material, *Energy Storage Science and Technology*, 39(2021), pp. 618-625, DOI No. 10.13941/j.cnki.21-1469/tk.2021.05.003.

[2] Mao, Q., Recent developments in geometrical configurations of thermal energy storage for concentrating solar power plant, *Renewable and Sustainable Energy Reviews*, 59(2016), pp.105833, DOI No. 10.1016/j.rser.2015.12.355.

[3] Leite da Cunha, S. R., Barroso de Aguiar, J. L., Phase change materials and energy efficiency of buildings: A review of knowledge, *Journal of Energy Storage*, 27(2020), pp. 101083, DOI No.10.1016/j.est.2019.101083.

[4] Dong, Y., *et al*., Review of latent thermal energy storage systems for solar air-conditioning systems, *International Journal of Energy Research*, 44(2020), pp. 669-707, DOI No. 10.1002/er.4960.

[5] Kalidasan, B., *et al*., Phase change materials integrated solar thermal energy systems: Global trends and current practices in experimental approaches, *Journal of Energy Storage*, 27(2020), pp. 101118, DOI No. 10.1016/j.est.2019.101118.

[6] Guelpa, E., Verda, V., Thermal energy storage in district heating and cooling systems: A review, *Applied Energy*, 252(2019), pp. 113474, DOI No. 10.1016/j.apenergy.2019.113474.

[7] Li, Z., *et al*., Applications and technological challenges for heat recovery, storage and utilisation with latent thermal energy storage, *Applied Energy*, 283(2021), pp. 116277, DOI No. 10.1016/j.apenergy.2020.116277.

[8] Moreno, P., *et al*., The use of phase change materials in domestic heat pump and air-conditioning systems for short term storage: A review, *Renewable & Sustainable Energy Reviews*, 39(2014), pp. 1-13, DOI No. 10.1016/j.rser.2014.07.062.

[9] Al-Aifan, B., *et al*., Performance evaluation of a combined variable refrigerant volume and cool thermal energy storage system for air conditioning applications, *International Journal of*

Refrigeration-Revue Internationale Du Froid, 76(2017), pp. 271-295, DOI No. 10.1016/j.ijrefrig.2017.02.008.

[10] Li, J., *et al*., Thermal performance of a plate-type latent heat thermal energy storage heat exchanger - An experimental investigation and simulation study, *Journal of Energy Storage*, 65(2023), pp.107295, DOI No. 10.1016/j.est.2023.107295.

[11] Zhu, X., et al., Heat transfer enhancement technology for fins in phase change energy storage, *Journal of Energy Storage*, 55(2022), pp.105833, DOI No. 10.1016/j.est.2022.105833

[12] Zhou, H. *et al*., Numerical simulation of internal heat transfer characteristics in a shell and tube cascade phase change heat storage device used in mariculture, *Journal of Dalian Ocean University*, 35(2020), pp. 599-606, DOI No. 10.16535/j.cnki.dlhyxb.2019-281.

[13] Yang, J., *et al*., Visualized experiment on dynamic thermal behavior of phase change material in metal foam, *CIESC Journal*, 68(2015), pp. 497-503, DOI No. 10.11949/j.issn.0438-1157.20141182.

[14] Wang, H., *et al*., Visualized experiment on solid-liquid phase change heat transfer enhancement with multiple PCMs, *CIESC Journal*, 70(2019), pp. 1263-1271+1662, DOI No. 10.11949/j.issn.0438-1157.20180936.

[15] Shafee, A., *et al*., Phase change process of nanoparticle enhanced PCM in a heat storage including unsteady conduction, *Journal of Molecular Liquids*, 309(2020), pp. 113102, DOI No. 10.1016/j.molliq.2020.113102.

[16] Kamkari, B., *et al*., Experimental investigation of the effect of inclination angle on convection-driven melting of phase change material in a rectangular enclosure, *International Journal of Heat and Mass Transfer*, 72(2014), pp. 186-200, DOI No. 10.1016/j.ijheatmasstransfer.2014.01.014.

[17] Gurel, B., Thermal performance evaluation for solidification process of latent heat thermal energy storage in a corrugated plate heat exchanger, *Applied Thermal Engineering*, 174(2020), pp. 115312, DOI No. 10.1016/j.applthermaleng.2020.115312.

[18] Lin, W., *et al*., Experimental study of the thermal performance of a novel plate type heat exchanger with phase change material, *Applied Thermal Engineering*, 178(2020), pp. 115630, DOI No. 10.1016/j.applthermaleng.2020.115630.

[19] Voller, V.R., Prakash, C., A fixed grid numerical modelling methodology for convection-diffusion mushy region phase-change problems, *Pergamon*, 30(1987), pp. 1709-1719, DOI No. 10.1016/0017-9310(87)90317-6.

[20] Voller, V. R., Swaminathan, C. R., Eral source-based method for solidification phase change. *Numerical Heat Transfer, Part B: Fundamentals*, 19(1991), pp. 175-189, DOI No. 10.1080/10407799108944962.

[21] Yuan, Y., *et al*., Melting Behaviors of Capric Acid in Rectangular Enclosure, *Journal of Southwest Jiaotong University*, 47(2012), pp. 236-240, DOI No. 10.3969/j.issn.0258-2724.2012.02.011.

Submitted: 28.08.2023.

Revised: 20.01.2024.

Accepted: 23.01.2024.